MIS18A upregulation promotes cell viability, migration and tumor immune evasion in lung adenocarcinoma

YONGJIE ZHU[1*], ZIHAO LI[2*], ZUOTAO WU[1*], TING ZHUO[3], LEI DAI[1], GUANBIAO LIANG[1], HUAJIAN PENG[1], HONGLIN LU[1] and YONGYONG WANG[1]

[1]Department of Cardio-Thoracic Surgery, The First Affiliated Hospital of Guangxi Medical University, Nanning, Guangxi Zhuang Autonomous Region 530021, P.R. China; [2]Department of Thoracic Surgery, Liuzhou People's Hospital Affiliated to Guangxi Medical University, Liuzhou, Guangxi Zhuang Autonomous Region 545026, P.R. China; [3]Department of Pulmonary and Critical Care Medicine, The First Affiliated Hospital of Guangxi Medical University, Nanning, Guangxi Zhuang Autonomous Region 530021, P.R. China

Received February 3, 2024; Accepted May 13, 2024

DOI: 10.3892/ol.2024.14509

Abstract. Lung adenocarcinoma (LUAD) presents a significant global health challenge owing to its poor prognosis and high mortality rates. Despite its involvement in the initiation and progression of a number of cancer types, the understanding of the precise impact of MIS18 kinetochore protein A (MIS18A) on LUAD remains incomplete. In the present study, the role of MIS18A in LUAD was investigated by analyzing the genomic and clinical data from multiple public datasets. The expression of MIS18A was validated using reverse transcription-quantitative polymerase chain reaction, and *in vitro* experiments involving small interfering RNA-induced downregulation of MIS18A in lung cancer cells were conducted to further explore its impact. These findings revealed that elevated MIS18A expression in LUAD was associated with advanced clinical features and poor prognosis. Functional analysis also revealed the role of MIS18A in regulating the cell cycle and immune-related pathways. Moreover, MIS18A altered the immune microenvironment in LUAD, influencing its response to immunotherapy and drug sensitivity. The results of the *in vitro* experiments indicated that suppression of MIS18A expression reduced the proliferative and migratory capacities of LUAD cells. In summary, MIS18A possesses potential as a biomarker and may serve as a possible therapeutic target for LUAD, with significant implications for tumor progression by influencing both cell cycle dynamics and immune infiltration.

Correspondence to: Professor Yongyong Wang, Department of Cardio-Thoracic Surgery, The First Affiliated Hospital of Guangxi Medical University, 6 Shuangyong Road, Nanning, Guangxi Zhuang Autonomous Region 530021, P.R. China
E-mail: wangyongyong@stu.gxmu.edu.cn

*Contributed equally

Key words: MIS18 kinetochore protein A, lung adenocarcinoma, prognostic biomarkers, cell cycle, immune infiltration

Introduction

Lung cancer is characterized by its extreme invasiveness and metastatic nature, contributing to the highest incidences of cancer and mortality rates worldwide (1). Histologically, lung cancer is categorized into two main types: Small cell lung cancer and non-small cell lung cancer, the latter of which represents ~85% of all cases (2), with lung adenocarcinoma (LUAD) emerging as the predominant subtype (3). The widespread adoption of low-dose computed tomography has notably increased the detection rate of lung cancer (4). However, despite recent advances in the diagnosis and treatment of lung cancer, a significant number of patients with LUAD ultimately succumb to the disease. Reports indicate a high mortality rate for LUAD, with a 5-year overall survival (OS) rate of <15% (5,6). Therefore, there is an urgent need to explore novel biomarkers and develop effective therapeutic approaches to improve the diagnosis and prognosis of patients with LUAD.

MIS18 Kinetochore Protein A (MIS18A), also known as Mis18α or C21orf45, is a crucial component of the Mis18 protein family, which also includes Mis18β and M18BP1. MIS18A is pivotal for the recruitment of centromere protein (CENP) A within the Mis18 complex and is essential for centromeric chromatin organization (7). MIS18A localizes to the centromere in a cell cycle-dependent manner, with its centromeric signals notably intensifying during a specific phase that spans from late anaphase-telophase to early G1, encompassing the post-segregation and pre-replication periods (8). Additionally, MIS18A and MIS18B form a heterotetramer complex through their C-terminal coiled-coil domains, which is pivotal for centromere recognition (9). CENPA, which encodes a centromeric protein with a histone fold domain closely related to histone H3, is crucial for the localization of this protein to the centromere (10). Elevated levels of CENPA have been identified as a potential diagnostic biomarker for LUAD and have been linked to poor OS rates (11). However, the precise roles and implications of MIS18A, which is intricately linked to CENPA expression, as well as the significance of the MIS18A complex in cancer, remain unclear. Nuclear MIS18A may function as a histone

modifier, potentially influencing chromatin hypermethylation through interactions with DNA methyltransferase (DNMT) 3A and DNMT3B (12). Furthermore, the upregulation of MIS18A has been linked to high microsatellite instability in colorectal cancer, highlighting the therapeutic potential of targeting autophagy protein 5-MIS18A or MIS18A, as their interaction promotes the hypermethylation of the hMLH1 promoter CpG island (13). Therefore, further exploration of the involvement of MIS18A in various cancer types is essential to comprehensively understand its clinical significance and potential mechanisms in diverse cancer types. The present study reports a primary effort to investigate MIS18A in the context of LUAD with the aim of unraveling its expression profile, prognostic relevance and underlying mechanisms.

Materials and methods

Data acquisition. Gene expression data, including LUAD mRNA count and Fragments Per Kilobase per Million mapped reads data, were collected from UCSC Xena (14) (https://xenabrowser.net/), for a cohort comprising 510 LUAD samples and 58 normal samples. This dataset also included clinical annotations and survival outcomes. To standardize the comparability and facilitate analysis, all data underwent a logarithmic transformation using the formula $\log_2(x+1)$. Long non-coding RNA (lncRNA), microRNA (miRNA) and nucleotide variation datasets pertinent to LUAD were obtained from The Cancer Genome Atlas (TCGA) database (https://portal.gdc.cancer.gov/). Additionally, the GSE30219 (15) (293 LUAD samples and 14 normal samples), GSE10072 (16) (58 LUAD samples and 49 normal samples) and GSE27262 (17) (25 LUAD tissues and 25 adjacent normal tissues) datasets were retrieved from the Gene Expression Omnibus (GEO) database (https://www.ncbi.nlm.nih.gov/geo/).

Discrepancies in MIS18A expression and its diagnostic potential in LUAD. This investigation focused on comparing the MIS18A expression levels between normal and tumor tissues based on data from TCGA and GEO databases. Patients with LUAD were categorized into low and high expression groups based on the median MIS18A expression level. The expression patterns of MIS18A across various cancer types were investigated using the TIMER database (18) (https://cistrome.shinyapps.io/timer/). The diagnostic utility of MIS18A in LUAD was assessed using Receiver Operating Characteristic (ROC) curve analysis. Validation of differential expression was conducted through reverse transcription-quantitative polymerase chain reaction (RT-qPCR) using our own collected samples (described later). The elevated MIS18A protein expression in LUAD was also confirmed through analysis of the Human Protein Atlas (HPA) (19) (http://www.proteinatlas.org/) and UALCAN (20) datasets (http://ualcan.path.uab.edu/).

Prognostic value analysis of MIS18A in LUAD. The prognostic significance of MIS18A in the TCGA-LUAD and GSE30219 cohorts was assessed using the R packages, 'survival' (version 3.6.4) (21) and 'survminer' (version 0.4.9) (22). Validation was conducted by analyzing the OS time using the Kaplan-Meier Plotter database (https://kmplot.com/analysis/) and the Gene Expression Profiling Interactive Analysis (GEPIA) dataset (23) (http://gepia.cancer-pku.cn/). Univariate and multivariate Cox proportional hazard regression analyses were performed to evaluate the independent prognostic significance of MIS18A in LUAD.

Identification of differentially expressed genes (DEGs) and functional enrichment analysis of MIS18A. Differential analysis of the TCGA dataset was performed using the 'DESeq2' (version 1.44.0) (24) package in R (version 4.2.2), where DEGs were characterized by genes with an absolute log2(fold change) >1 and adjusted $P<0.05$. The identification of these DEGs was visually depicted through Volcano plots. Subsequently, the Weighted Gene Co-expression Network Analysis (WGCNA) method, implemented via the R package 'WGCNA', was used to identify gene modules correlated with the expression of the MIS18A gene (25). The resultant gene module underwent enrichment analyses, including Gene Ontology (GO), Kyoto Encyclopedia of Genes and Genomes (KEGG) and Gene Set Enrichment Analysis (GSEA). To comprehensively elucidate the biological functions associated with MIS18A, enrichment analyses were performed using the R packages, 'clusterProfiler' (version 4.12.0) and 'org.Hs.eg.db' (version 3.19.1).

Diagnostic value and survival analysis of the hub Genes. During the GSEA, 6 hub genes were identified through the intersection of the protein-protein interaction (PPI) network associated with MIS18A, obtained from the GeneMANIA (26) database (http://www.genemania.org), with the turquoise module. Subsequently, a comprehensive investigation into the diagnostic and prognostic significance of these hub genes was conducted, as aforementioned.

Immune infiltration analysis of MIS18A in LUAD. The ESTIMATE algorithm (27) was used to calculate estimate scores, immune scores, stromal scores and tumor purity for LUAD samples. Subsequently, the differences in these scores between samples with high and low MIS18A expression were analyzed. The single-sample GSEA (ssGSEA) algorithm, implemented through the 'GSVA' package (version 1.52.2) (28), was adopted to evaluate 28 subtypes of immune cells in LUAD. Additionally, the relationship between MIS18A and chemokines, as well as chemokine receptors, was explored using the Tumor-Immune System Interaction Database (TISIDB; http://cis.hku.hk/TISIDB/index.php).

Examination of the correlation between tumor mutation burden (TMB) and drug sensitivity with MIS18A in LUAD. The 'maftools' package (version 2.20.0) was utilized for the comprehensive analysis and visualization of Mutation Annotation Format data (29). The Spearman's correlation coefficient test was used to examine the correlation between MIS18A and TMB. To predict the potential efficacy of chemotherapy and targeted treatments for LUAD cases with upregulated MIS18A, semi-inhibitory concentration (IC_{50}) data were obtained from the Genomics of Drug Sensitivity in Cancer database (https://www.cancerrxgene.org/) (30). The analysis was conducted using the 'OncoPredict' (version 1.2) (31), 'ggpubr' (version 0.6.0) and 'ggplot2' (version 3.5.1) packages within the R software.

Pathological sample collection. The samples and data from 30 pathological LUAD cases were collected from the First Affiliated Hospital of Guangxi Medical University (Nanning, China). A total of 30 LUAD and 30 adjacent non-cancerous tissue samples were collected from July 2022 to September 2022. The included patients comprised 15 males and 15 females, with an average age of 63 years and an age range of 32 to 78 years. The inclusion criteria required patients to have undergone surgical treatment at the First Affiliated Hospital of Guangxi Medical University and to have received a confirmed pathological diagnosis of LUAD. Patients with other types of lung cancer or immune system disorders, or those who had received chemotherapy or radiation therapy before surgery were excluded from the present study. All participants provided written informed consent, and the study protocol was approved by the Ethics Committee of the First Affiliated Hospital of Guangxi Medical University, guaranteeing adherence to strict ethical standards to protect patient privacy and rights. These meticulous data collection methods and ethical considerations have established a solid foundation for the subsequent data analysis in this study.

Cell culture and RNA interference. The A549 LUAD cell line was obtained from The Cell Bank of Type Culture Collection of The Chinese Academy of Sciences. These cells were cultured in Dulbecco's Modified Eagle Medium (DMEM) supplemented with 10% fetal bovine serum (FBS) and 1% penicillin and streptomycin (all sourced from Gibco; Thermo Fisher Scientific, Inc.), and were maintained at 37˚C in a 5% CO_2 atmosphere. Lipofectamine® 8000 (Beyotime Institute of Biotechnology) was used to transfect small interfering RNA (siRNA) into the cells in a serum-free culture medium according to the manufacturer's instructions. For the CCK-8 assay performed in a 96-well plate, 5 μl serum-free medium, 4 pmol siRNA and 0.16 μl Lipofectamine 8000 transfection reagent were used. For the wound healing and Transwell invasion assays performed in 6-well plates, 125 μl serum-free medium, 100 pmol siRNA and 4 μl Lipofectamine 8000 transfection reagent were used. After adding siRNA, the mixture was gently mixed, followed by the addition of Lipofectamine 8000 transfection reagent and gentle mixing again. The mixtures were incubated at room temperature for 20 min before adding to the cells. The cells were then incubated at 37˚C in a 5% CO_2 atmosphere for 2 days before subsequent experiments. Specific details regarding the siRNA sequences can be found in Table I.

RNA extraction and RT-qPCR. The aforementioned patient tissue samples were immediately flash-frozen in liquid nitrogen upon collection and subsequently stored at -80˚C. Total RNA was extracted from these samples using RNAiso Plus (Takara Bio, Inc.) at 4˚C. cDNA was synthesized from 1.0 μg total RNA using the Prime Script RT Master Mix (Takara Bio, Inc.), as per the manufacturer's instructions. qPCR was conducted using the Fast Start Universal SYBR Green Master (Roche Diagnostics) and 2X Q3 SYBR qPCR Master Mix (Tolo Biotech Co., Ltd.) to quantify gene expression. The amplification protocol involved an initial denaturation at 95˚C for 30 sec, followed by 40 cycles of 95˚C for 10 sec and 60˚C for 30 sec. Relative gene expression was determined using the $2^{-\Delta\Delta Cq}$ method (17), with GAPDH as the normalization control. The primer sequences (synthesized by Nanning Genesis Biotechnology Co., Ltd.) were as follows: GAPDH forward, 5'-GCACCGTCAAGGCTGAGAAC-3' and reverse, 5'-ATGGTGGTGAAGACGCCAGT-3'; and MIS18A forward, 5'-TGCTTCGCTGTGTTTCCTGT-3' and reverse, 5'-TGACACAATTTGCTTTTCAGAGGAC-3'. The same protocol was followed for the MIS18A siRNA-transfected cells.

Table I. siRNA sequences.

Primer	Sequence (5'-3')
si-NC	UUCUCCGAACGUGUCACGU
si-MIS18A-1	GCCGAAUCCAAAUUGUCCUUU
si-MIS18A-2	GCCCAAGAAUCUUGAUUACAA
si-MIS18A-3	CUUCGCUGUGUUUCCUGUAAU

siRNA, small interfering RNA; MIS18A, MIS18 kinetochore protein A; NC, negative control.

Cell Counting Kit-8 (CCK-8) assay. The transfected cells were seeded into 96-well plates and incubated for 48 h. Subsequently, 10 μl CCK-8 reagent (Dojindo Laboratories, Inc.) was added to each well, and the cells were incubated at 37˚C for 2 h. The absorbance at 450 nm was measured using a microplate reader (Thermo Fisher Scientific, Inc.).

Wound healing assay. Cells were seeded into 6-well plates and transfected upon reaching 80-90% confluency. A precise vertical wound was created using a sterile 200 μl pipette tip. The plate was subsequently washed with phosphate buffered saline to remove any detached cells, then further cultured in serum-free medium. Images were collected at 0, 24 and 48 h following wounding using a light microscope (Nikon Corporation), and the wound closure rate was subsequently analyzed by measuring the wound area at each time point using ImageJ (version 1.53q; National Institutes of Health) software and calculating the percentage of wound closure at 24 and 48 h relative to the initial wound area at 0 h.

Transwell invasion assay. Invasion assays were performed using Transwell plates with a 8-μm pore size (LabSelect; Beijing Lanjieke Technology Co., Ltd.). The Transwell chambers were precoated with Matrigel; all operations were carried out on ice, and all pipette tips were pre-cooled. Matrigel was diluted with serum-free culture medium at a ratio of 9:1 (culture medium:Matrigel) and mixed thoroughly. Matrigel mixture (100 μl) was carefully added to the polycarbonate membrane in each Transwell chamber, forming a layer of artificial extracellular matrix while avoiding bubbles. The chambers were then incubated at 37˚C for 2 h to allow the Matrigel to solidify. Cells, collected 24 h after transfection, were resuspended and 200 μl containing 20,000 cells was placed into the upper chamber of the Transwell plate. The lower chamber contained 500 μl DMEM supplemented with 10% FBS. The cells were then incubated at 37˚C for 24 h. Following incubation, the

cells were stained with crystal violet (Beyotime Institute of Biotechnology) for 10 min at room temperature and quantified in various randomly selected regions using a light microscope (Nikon Corporation).

Construction of the competing endogenous RNA (ceRNA) network for MIS18A. An analysis using the ENCORI database (https://starbase.sysu.edu.cn/) was performed to predict non-coding RNAs that may regulate MIS18A expression through the ceRNA mechanism. The criteria for miRNA selection included a Spearman's correlation coefficient of <-0.2 and P<0.05, enabling the identification of miRNAs targeting MIS18A. Subsequently, emphasis was placed on miRNAs that were downregulated in LUAD and exhibited a positive correlation with patient prognosis. Regarding lncRNAs, two criteria were employed: Spearman's correlation coefficient of <-0.2 and P<0.05 for a negative correlation with miRNA, and a Spearman's correlation coefficient of >0.2 and P<0.05 for a positive correlation with mRNA. lncRNAs meeting these criteria were considered as those that target MIS18A, while those upregulated in LUAD with a negative correlation with patient prognosis were identified as core lncRNAs associated with MIS18A.

Statistical analysis. Statistical analyses were performed using R (version 4.2.2) and GraphPad Prism (version 7.0; Dotmatics). Differential expression analysis between two groups was performed using the Wilcoxon rank-sum test. Survival analysis was conducted using the Kaplan-Meier method to plot survival curves, with the log-rank test to assess differences between groups. For cases where survival curves exhibited late crossover, the two-stage method provided by the 'TSHRC' package (version 0.1.6) was employed for further comparison. Univariate and multivariate Cox regression analyses were used to identify independent prognostic factors. Correlation analysis was conducted using the Spearman's correlation test. Multiple group comparisons were conducted using one-way ANOVA followed by the Tukey post hoc test. Each assay was replicated in at least three independent experiments. P<0.05 was considered to indicate a statistically significant difference.

Results

Diagnostic potential of MIS18A in LUAD. Pan-cancer expression analysis using the TIMER database revealed a significant increase in MIS18A mRNA expression in 19 different cancer tissue types (Fig. 1A). Analysis of the TCGA dataset and validation across three GEO datasets confirmed the upregulation of MIS18A in LUAD (Fig. 1B-E). Furthermore, the differential expression of MIS18A in LUAD was validated using RT-qPCR with tissue samples collected from patients at the First Affiliated Hospital of Guangxi Medical University (Fig. 1J). The area under the curve (AUC) values were 0.962 for the TCGA dataset and 0.917, 0.890 and 0.971 for the GSE30219, GSE10072 and GSE27262 GEO datasets, respectively (Fig. 1F-I), suggesting that MIS18A could serve as a reliable diagnostic marker for LUAD. Examination using the HPA (Fig. 1K) and UALCAN (Fig. 1L) databases revealed a significant upregulation of MIS18A protein expression in LUAD samples.

Prognostic significance of MIS18A in LUAD. Next, the correlation between MIS18A expression and various clinical characteristics, including prognosis and tumor (T) and node stage were investigated. Analysis of the TCGA cohort indicated that high MIS18A expression was correlated with a poorer prognosis (Fig. 2A). This association was validated following analyses of the GSE30219 dataset (Fig. 2B) and GEPIA (Fig. 2C) and Kaplan-Meier Plotter (Fig. 2D) databases. Within the TCGA-LUAD cohort, both the Cox univariate (Fig. 2E) and multivariate (Fig. 2F) analyses demonstrated that MIS18A expression could independently predict a poor prognosis [hazard ratio (HR)>1; P<0.05]. Moreover, elevated MIS18A expression was detected in patients with LUAD who exhibited a higher clinical T stage (Fig. 2G), the presence of lymph node metastases (Fig. 2H) and advanced pathological stages (Fig. 2I).

Identification of DEGs and enrichment analysis to explore MIS18A-related signaling pathways in LUAD. To investigate the potential roles of MIS18A in LUAD, 788 upregulated and 473 downregulated DEGs were identified by analyzing the gene expression profiles from TCGA database (Fig. 3A). Cluster analysis of these genes can provide insights into the functions of MIS18A. Utilizing the average linkage hierarchical clustering method, DEGs were effectively classified into five modules (Fig. 3B-E). The heatmap revealed that the genes within the turquoise module (n=899) exhibited a strong positive correlation with MIS18A expression (ρ=0.76; P=4x10^{-98}) and a weak correlation with tumor purity (ρ=0.24; P=4x10^{-8}). Additionally, MIS18A expression was negatively correlated with the immune score (ρ=-0.22; P=7x10^{-7}) (Fig. 3F). Subsequent functional enrichment analysis of the turquoise module genes identified significant associations with the cell cycle and metabolic pathways (Fig. 3G). These included terms such as 'nuclear division', 'chromosome segregation', 'chromosomal region', 'DNA-binding transcription activator activity', 'single-stranded DNA helicase activity', 'Cell cycle' and 'neuroactive ligand-receptor interaction'. Additionally, GSEA highlighted the involvement of genes from the turquoise module in a variety of biological terms, including 'GO_CELL_SURFACE', 'GO_CYTOPLASMIC_VESICLE_PART', 'GO_DNA_BINDING_TRANSCRIPTION_FACTOR_ACTIVITY', 'GO_IMMUNE_EFFECTOR_PROCESS','GO_POSITIVE_REGULATION_OF_IMMUNE_SYSTEM_PROCESS', 'GO_REGULATION_OF_IMMUNE_RESPONSE', 'GO_REGULATION_OF_IMMUNE_SYSTEM_PROCESS', 'GO_REGULATORY_REGION_NUCLEIC_ACID_BINDING', 'GO_SEQUENCE_SPECIFIC_DNA_BINDING' and 'GO_VACUOLE' (Fig. 3H). These terms were primarily associated with cell cycle and immune-related pathways. Enrichment analysis therefore suggested that MIS81A may promote cell division and influence the tumor immune microenvironment.

Identification and analysis of the diagnostic and prognostic value of the hub genes. To investigate the relationship between MIS18A and other genes, the MIS18A PPI network was examined using GeneMANIA, which predicted its interactions with 20 proteins. These proteins collectively form a multifaceted PPI network characterized by physical interactions,

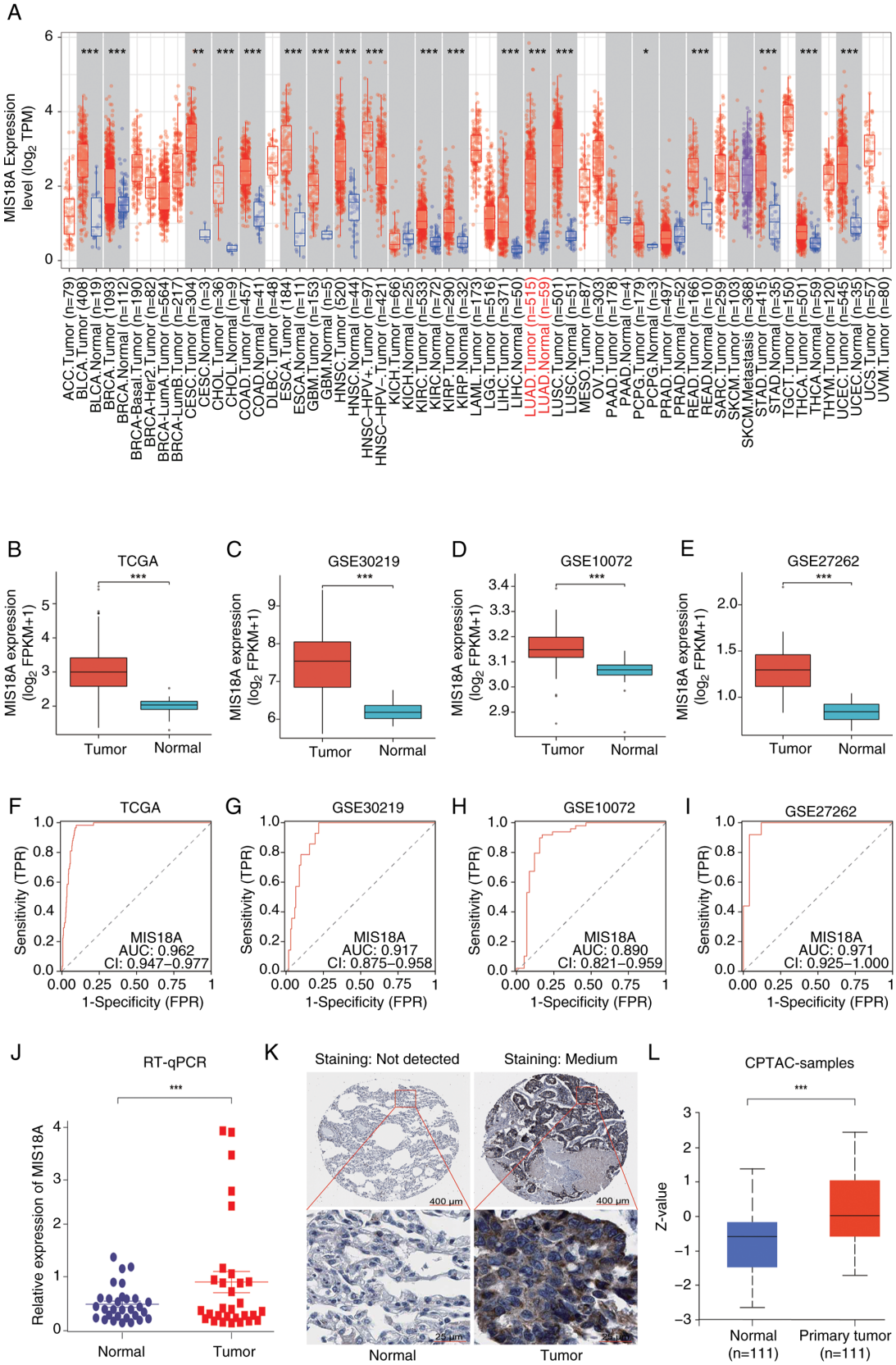

Figure 1. MIS18A upregulation in LUAD and its diagnostic significance. (A) Data regarding the upregulation of MIS18A mRNA levels in various malignancies, including LUAD, was retrieved from the TIMER database. Comparative analysis of MIS18A between tumor and normal groups in (B) TCGA and three GEO datasets, (C) GSE30219, (D) GSE10072 and (E) GSE27262. Diagnostic Receiver Operator Characteristic curve analysis of MIS18A in (F) TCGA and the three GEO datasets, (G) GSE30219, (H) GSE10072 and (I) GSE27262. (J) Comparison of MIS18A expression levels between tumor and adjacent lung tissues using RT-qPCR. (K) Representative immunohistochemistry images of MIS18A in LUAD and normal lung tissues from the Human Protein Atlas database. (L) Upregulation of MIS18A protein levels in LUAD tissues according to UALCAN. *P<0.05, **P<0.01, ***P<0.001. LUAD, lung adenocarcinoma; MIS18A, MIS18 kinetochore protein A; TCGA, The Cancer Genome Atlas; GEO, Gene Expression Omnibus; TPM, transcripts per million; FPKM, Fragments Per Kilobase per Million mapped reads; TPR, true-positive rate; FPR, false-positive rate; CPTAC, Clinical Proteomic Tumor Analysis Consortium; AUC, area under the curve; CI, confidence interval; RT-qPCR, reverse transcription-quantitative PCR.

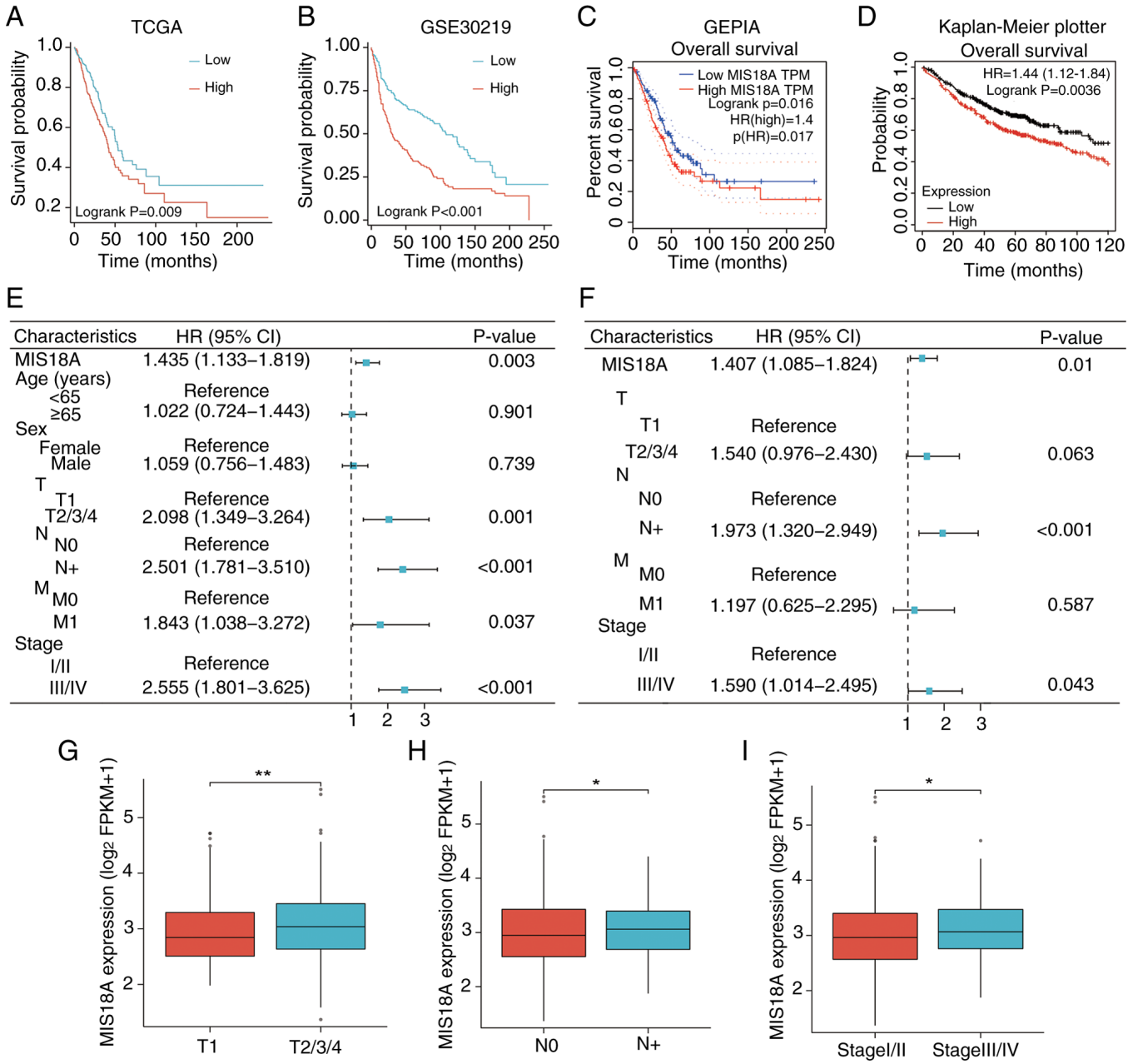

Figure 2. Correlation of upregulated MIS18A expression with poor prognosis. Kaplan-Meier survival analysis comparing distinct MIS18A expression levels in the (A) TCGA and (B) GSE30219 datasets. (C) Kaplan-Meier survival curve of MIS18A from the GEPIA database. (D) Kaplan-Meier survival curve of MIS18A from the Kaplan-Meier Plotter database. (E) Univariate and (F) multivariate Cox regression analysis using the TCGA dataset. Association of the MIS18A mRNA levels in samples from patients across various (G) clinical T, (H) N and (I) pathological stages. *P<0.05, **P<0.01. TCGA, The Cancer Genome Atlas; GEPIA, Gene Expression Profiling Interactive Analysis; T, tumor; N, node; M, metastasis; TPM, transcripts per million; FPKM, Fragments Per Kilobase per Million mapped reads; HR, hazard ratio; CI, confidence interval; MIS18A, MIS18 kinetochore protein A.

co-expression patterns, predicted interactions, co-localization, genetic interactions and pathway associations. These proteins were implicated in various biological processes, including 'CENP-A containing chromatin organization', 'DNA replication-independent nucleosome assembly', 'chromatin remodeling at centromere', 'histone exchange', 'DNA replication-independent nucleosome organization', 'centromere complex assembly' and 'nucleosome assembly' (Fig. 4A). Overlapping the PPI network with genes from the turquoise module identified 6 DEGs, namely MIS18A, Holliday junction recognition protein (HJURP), Opa interacting protein 5 (OIP5), CENPA, CENPK and CENPU, as hub genes (Fig. 4B). Subsequent analyses of these hub genes were performed. Cox analysis identified all hub genes as risk factors (HR >1; Fig. 4C), contributing to an unfavorable prognosis in LUAD. This was further corroborated by the Kaplan-Meier survival analysis using the GEPIA database (Fig. 4N-R). Additionally, the hub genes were found to be upregulated in tumor tissues (Fig. 4D-H). ROC curves were generated using the TCGA cohort to evaluate the diagnostic efficacies of HJURP, OIP5, CENPA, CENPK and CENPU for LUAD, with corresponding AUCs of 0.984, 0.949, 0.967, 0.943 and 0.958, respectively (Fig. 4I-M). These results demonstrated the notable diagnostic potential of the hub genes identified in LUAD.

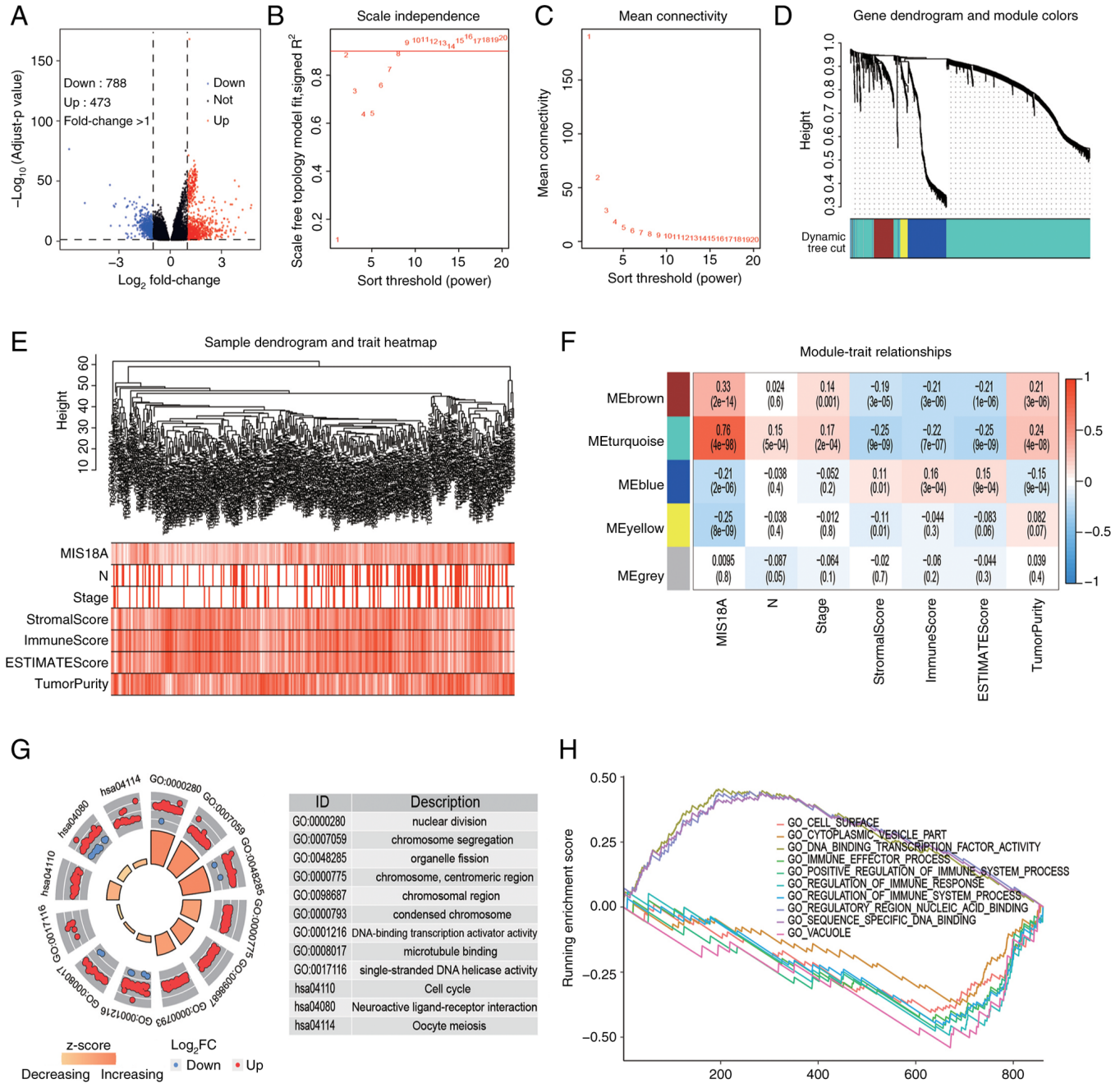

ID	Description
GO:0000280	nuclear division
GO:0007059	chromosome segregation
GO:0048285	organelle fission
GO:0000775	chromosome, centromeric region
GO:0098687	chromosomal region
GO:0000793	condensed chromosome
GO:0001216	DNA-binding transcription activator activity
GO:0008017	microtubule binding
GO:0017116	single-stranded DNA helicase activity
hsa04110	Cell cycle
hsa04080	Neuroactive ligand-receptor interaction
hsa04114	Oocyte meiosis

Figure 3. DEGs and functional analysis of MIS18A. (A) Volcano plot displaying the significant DEGs in The Cancer Genome Atlas dataset. (B) Scale-free fitting index calculation with various soft thresholds (power). (C) Analysis of mean connectivity at various soft thresholds (power). (D) Gene dendrogram showing LUAD sample clustering. (E) Composite graph showing LUAD sample clustering and correlations with clinical parameters. (F) Heatmap depicting the relationship between gene modules and clinical parameters. (G) Results of the GO and Kyoto Encyclopedia of Genes and Genomes analyses with turquoise module genes presented in a circular diagram. (H) Gene Set Enrichment Analysis results for the turquoise module genes. DEG, differentially expressed genes; LUAD, lung adenocarcinoma; GO, Gene Ontology; N, lymph node metastases; FC, fold change; MIS18A, MIS18 kinetochore protein A.

Relationship between MIS18A and the tumor microenvironment (TME). The TME plays a crucial role in clonal evolution, growth, metastasis, prognosis, drug resistance and tumor treatment outcomes. Consequently, the immune characteristics of MIS18A in LUAD were analyzed. The ESTIMATE algorithm was used to calculate the stromal, immune and ESTIMAE scores, which were subsequently used to estimate tumor purity. The results indicated that elevated MIS18A expression was associated with a significant decrease in the ESTIMATE (Fig. 5A), immune (Fig. 5B) and stromal (Fig. 5C) scores, which was accompanied by a higher tumor purity (Fig. 5D). The ssGSEA revealed a significant increase in the enrichment of activated $CD4^+$ T cells, memory B cells and Type 2 T helper cells in the high MIS18A expression group. By contrast, the low MIS18A expression group exhibited higher enrichment levels in 19 immune cell subtypes, including activated B cells, activated dendritic cells (DCs), central memory $CD4^+$ T cells and natural killer cells (Fig. 5E). Furthermore, MIS18A expression demonstrated positive correlations with activated $CD4^+$ T cells (ρ=0.34; P<0.001), memory B cells (ρ=0.24; P<0.001) and Type 2 T helper cells (ρ=0.13; P=0.003), but negative correlations with mast cells (ρ=-0.42; P<0.001), eosinophils (ρ=-0.39;

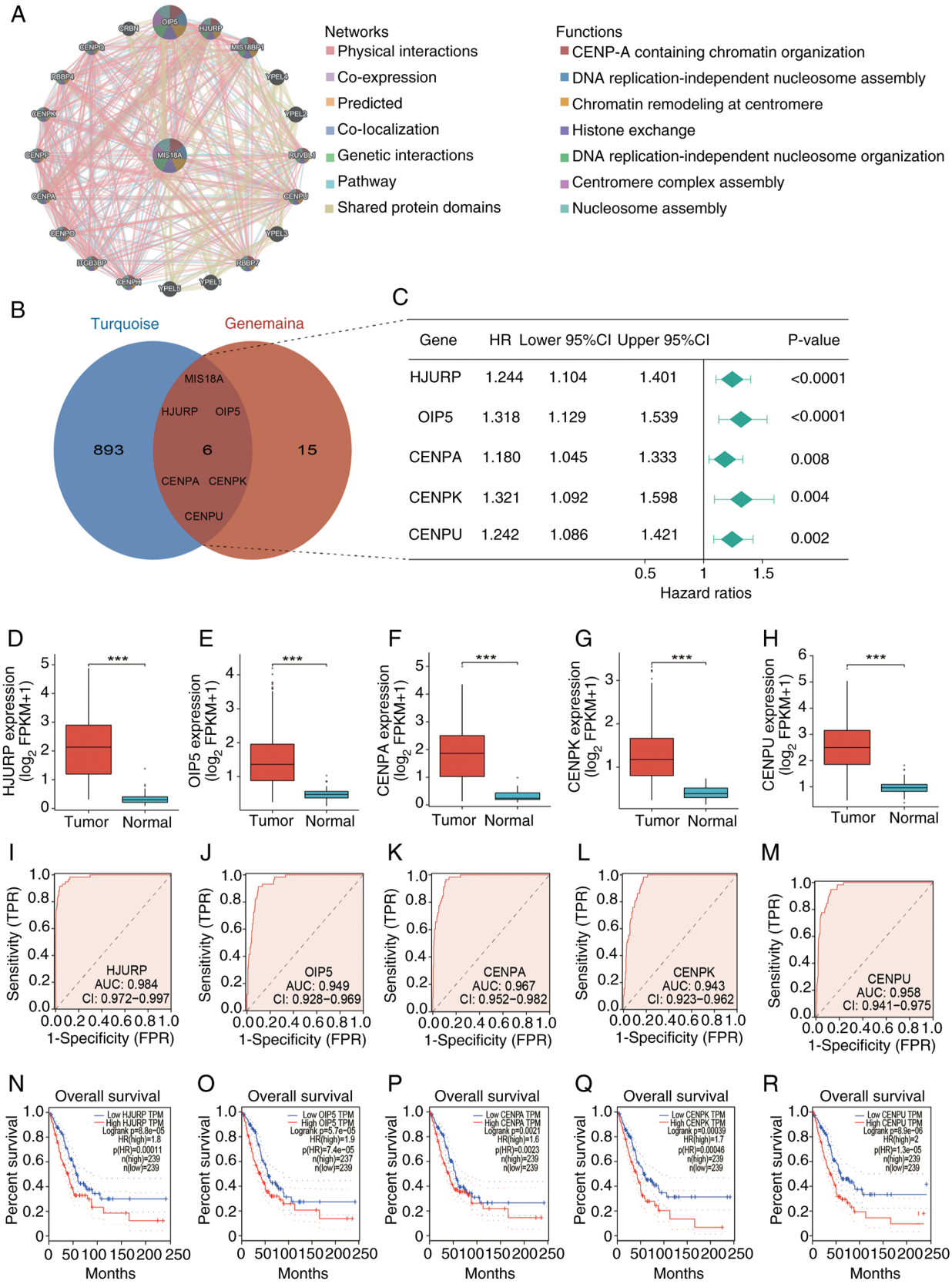

Figure 4. Identification of hub genes and their diagnostic and prognostic value in LUAD. (A) Protein-protein interaction network of MIS18A with interactive genes from the GeneMANIA database. Each point represents a gene. In the network section, green lines represent genetic interactions and in the functions section, the green parts within the genes signify DNA replication-independent nucleosome organization. (B) Identification of the 6 hub genes: MIS18A, HJURP, OIP5, CENPA, CENPK and CENPU. (C) Forest plot of Cox analysis of the hub gene expression. (D-H) Differential expression of the hub genes between tumor and normal groups. (I-M) Diagnostic Receiver Operator Characteristic curves of the hub genes for differentiating LUAD from normal tissue. (N-R) High expression of the hub genes was associated with decreased overall survival in patients with LUAD from the Gene Expression Profiling Interactive Analysis database. ***P<0.001. LUAD, lung adenocarcinoma; MIS18A, MIS18 kinetochore protein A; HJURP, holliday junction recognition protein; OIP5, Opa interacting protein 5; CENPA, centromere protein A; HR, hazard ratio; CI, confidence interval; AUC, area under the curve; FPR, false-positive rate; TPR, true-positive rate.

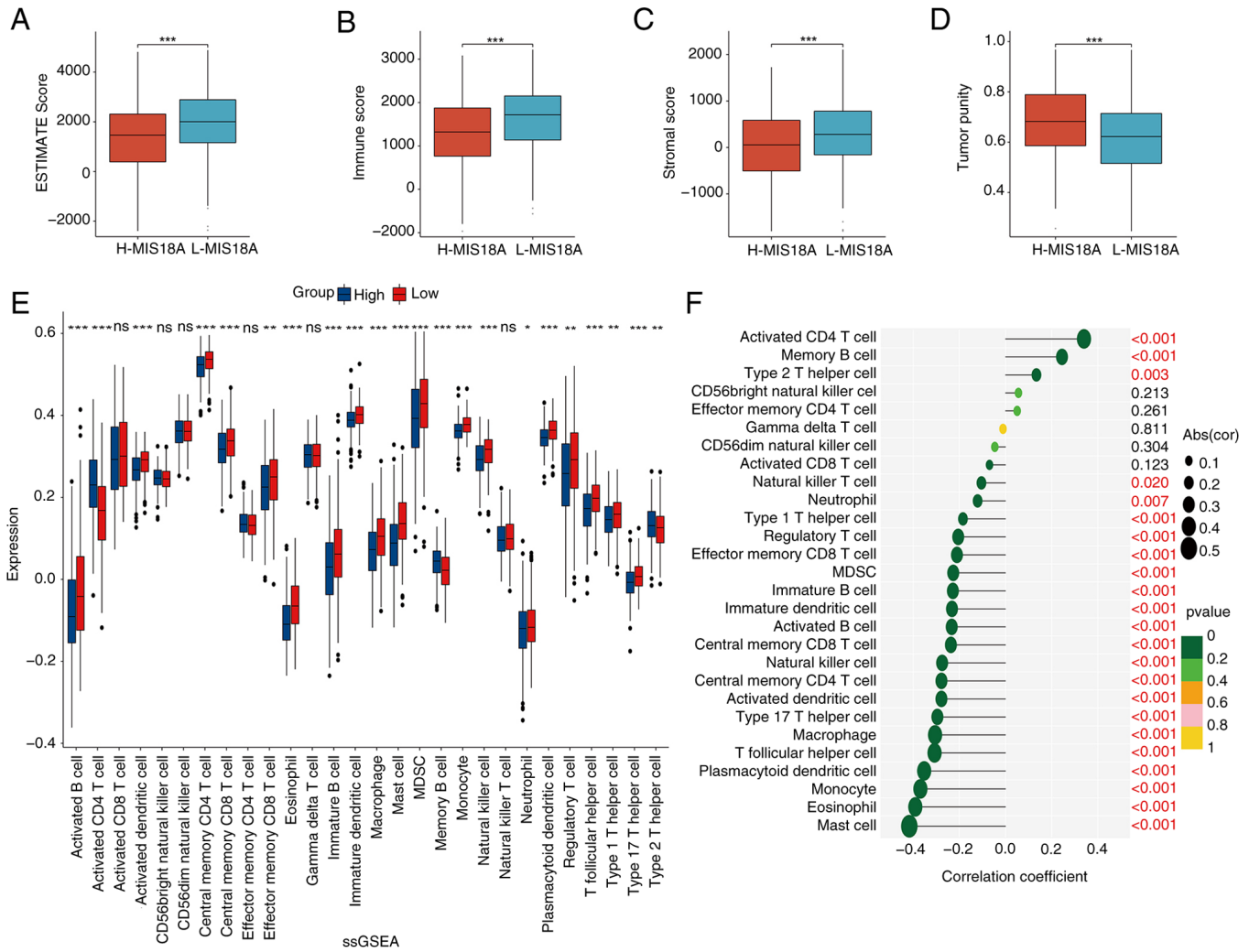

Figure 5. Relationship between MIS18A expression and the tumor microenvironment. Comparison of the (A) ESTIMATE, (B) immune, (C) stromal and (D) tumor purity score between groups with different levels of MIS18A expression. (E) Comparison of immune cell expression between groups with different levels of MIS18A expression using ssGSEA. (F) Correlation of MIS18A expression with 28 types of tumor-infiltrating immune cells based on ssGSEA. *P<0.05, **P<0.01, ***P<0.001. ssGSEA, single-sample Gene Set Enrichment Analysis; MIS18A, MIS18 kinetochore protein A; H-, high (expression); L-, low (expression); ns, not significant.

P<0.001), monocytes (ρ=-0.37; P<0.001) and plasmacytoid DCs (ρ=-0.35; P<0.001), among others (Fig. 5F). Additionally, analysis of the TISIDB revealed a negative correlation between MIS18A and various immune-related chemokines, further substantiating the role of MIS18A as an immune regulator in LUAD (Fig. S1).

Mutation analysis and assessment of drug sensitivity benefits. To assess the correlation between MIS18A expression and the immune therapeutic response, gene mutation maps for different MIS18A expression groups were presented using a waterfall plot. Elevated MIS18A expression was associated with an increased frequency of TP53 and TTN mutations (Fig. 6A). Moreover, the high MIS18A expression cohort demonstrated a significantly higher TMB and a robust correlation between MIS18A expression and the TMB (P<0.01; Fig. 6B and C). With the view of improving treatment outcomes for patients with LUAD, variations in sensitivity to commonly used chemotherapeutic agents and targeted drugs between the high and low MIS18A expression groups were meticulously examined. The results demonstrated that the high MIS18A expression group displayed a lower IC_{50} value than the low MIS18A expression group in response to cisplatin, paclitaxel, gefitinib and erlotinib (Fig. 6D).

Experimental verification. Based on the aforementioned evidence suggesting the potential involvement of MIS18A in LUAD progression, gene knockdown experiments were conducted in A549 cells. Initially, knocking down MIS18A at three distinct sites significantly reduced its expression, consequently leading to the selection of si-MIS18A-2 for further experiments (Fig. 7A). Subsequent analysis using the CCK-8 assay demonstrated a significant reduction in A549 cell viability at 48 h after MIS18A downregulation (Fig. 7B). Furthermore, the results of the wound healing assay revealed a significant inhibition of A549 cell migration following MIS18A knockdown (Fig. 7C). Finally, the Transwell invasion assay demonstrated a significant reduction in A549 cell invasion following MIS18A knockdown (Fig. 7D). Collectively, these results confirmed a reduction in cellular viability,

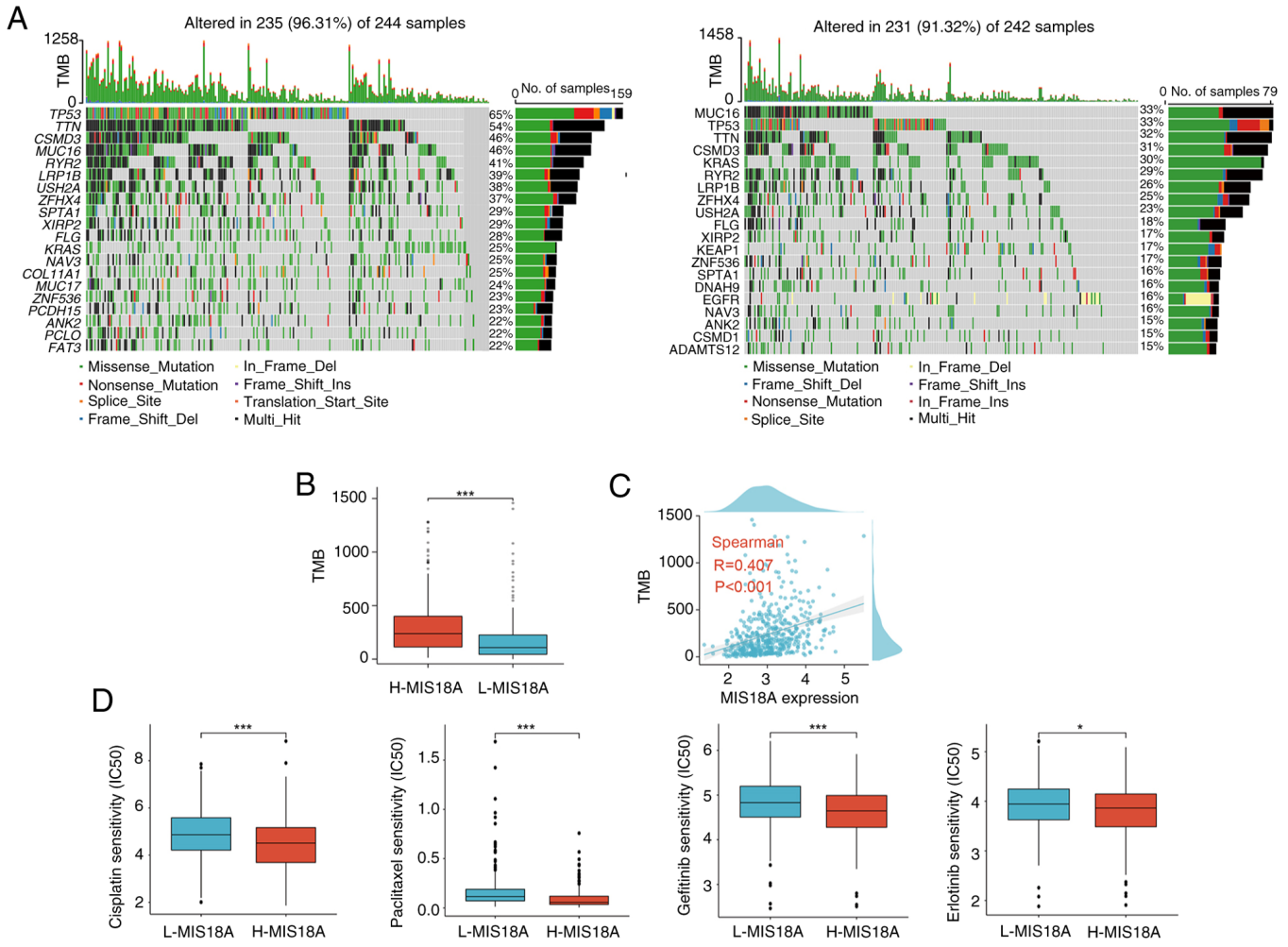

Figure 6. Influence of MIS18A on drug sensitivity in LUAD. (A) Gene mutation profiles across different MIS18A groups. (B) Differential analysis of the TMB between the high and low MIS18A expression groups in LUAD. (C) Relationship between MIS18A and TMB in LUAD. (D) Effect of MIS18A expression on IC_{50} values of first-line therapeutic drugs in LUAD. *P<0.05, ***P<0.001. LUAD, lung adenocarcinoma; MIS18A, MIS18 kinetochore protein A; H-, high (expression); L-, low (expression); TMB, tumor mutational burden.

migration and invasion upon transfection and subsequent gene knockdown with si-MIS18A.

Establishment of a ceRNA network associated with MIS18A. The aforementioned findings suggested that MIS18A enhances the viability, migration and invasion of LUAD cells, prompting an in-depth investigation into its multifaceted nature. Increasing evidence suggests that alterations and dysfunctions in lncRNAs contribute to abnormal gene expression and promote the development, progression and metastasis of various cancer types (32,33). lncRNAs sequester miRNAs, thereby influencing their mRNA expression (34). Therefore, a ceRNA regulatory network of MIS18A in LUAD was constructed to explore the relationships between MIS18A, lncRNAs and miRNAs. The three predicted miRNAs in the network demonstrated correlation coefficients with MIS18A expression of approximately-0.3, indicating a weak correlation (Fig. 8A-C). Despite this, hsa-miR-101-3p was selected as the principal miRNA for further study, primarily due to its observed upregulation in lung tissues (Fig. 8F) and the association of high hsa-miR-101-3p expression with a favorable prognosis in patients (Fig. 8H), underscoring its significant biological relevance in LUAD. GSEC, the lncRNA predicted by hsa-miR-101-3p, showed an inverse correlation with hsa-miR-101-3p (Fig. 8D) and a positive correlation with MIS18A (Fig. 8E). The upregulation of GSEC in LUAD demonstrated a significant association with an unfavorable prognosis (Fig. 8G and I), resulting in the identification of GSEC as the principal lncRNA in the ceRNA network associated with MIS18A in LUAD.

Discussion

Lung cancer is a common and lethal malignancy worldwide (35). The emergence of precision medicine has steered tumor treatment strategies towards minimally invasive, efficient and personalized approaches, progressively advancing cancer therapeutics (36). In terms of advancement in cancer research, Wang *et al* (37) demonstrated the development of integrative serum metabolic fingerprint-based multimodal platforms designed for lung nodule characterization and the early detection of LUAD. Another study underscored the innovative application of mass spectrometry/spectroscopy and machine learning in *in vitro* diagnostics, demonstrating

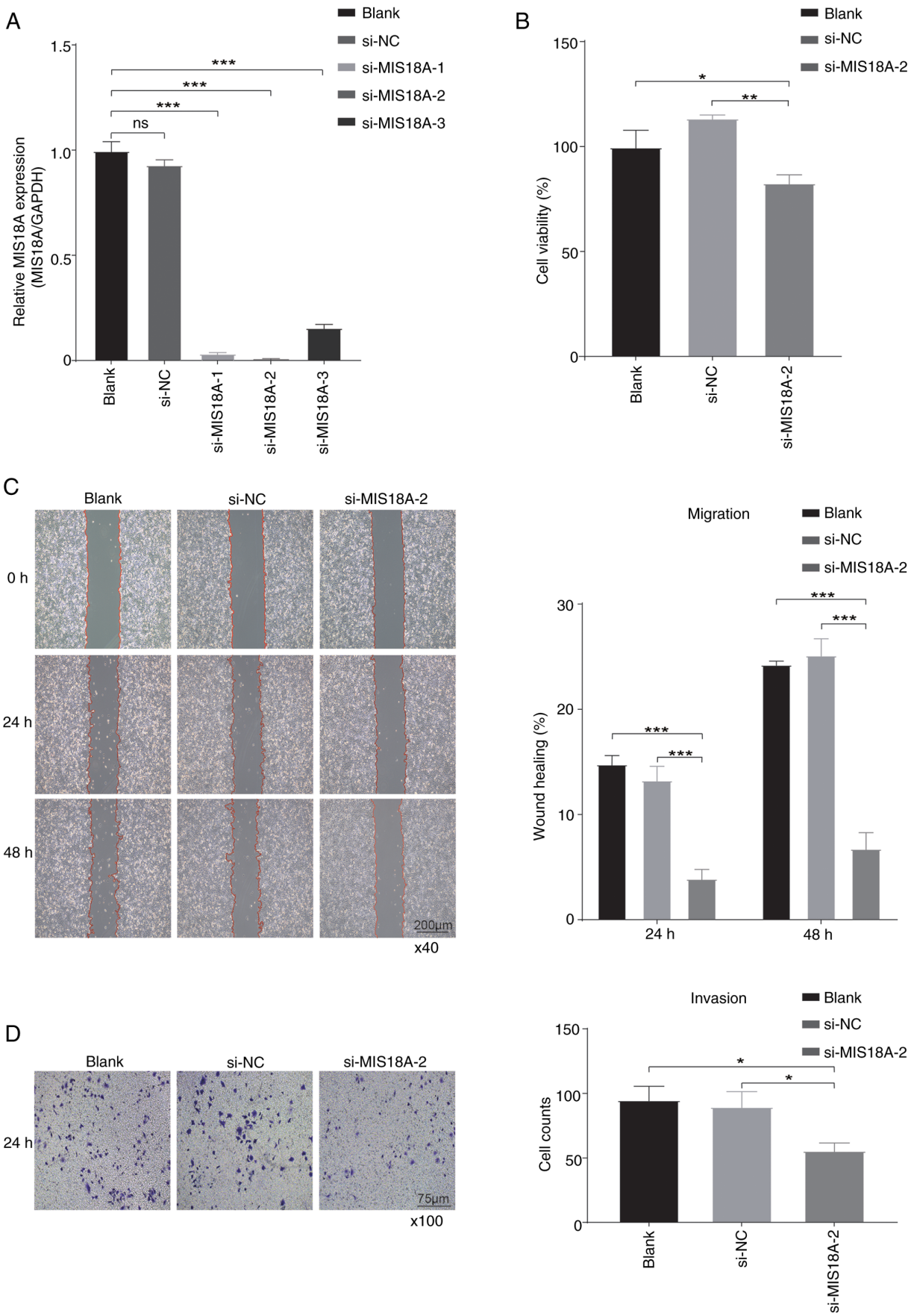

Figure 7. Suppression of cell proliferation, migration and invasion by MIS18A knockdown in LUAD. (A) MIS18A mRNA expression in A549 cells following transfection with si-MIS18A. (B) Cell Counting Kit-8 assay showing a reduction in LUAD cell viability following transfection with si-MIS18A-2. (C) Wound healing assays revealed a decrease in the wound healing rate of LUAD cells following transfection with si-MIS18A-2. Magnification, x40. (D) Transwell assays showing the suppression of LUAD cell invasion following transfection with si-MIS18A-2. Magnification, x100. *P<0.05, **P<0.01, ***P<0.001. LUAD, lung adenocarcinoma; MIS18A, MIS18 kinetochore protein A; si, small interfering; NC, negative control; ns, not significant.

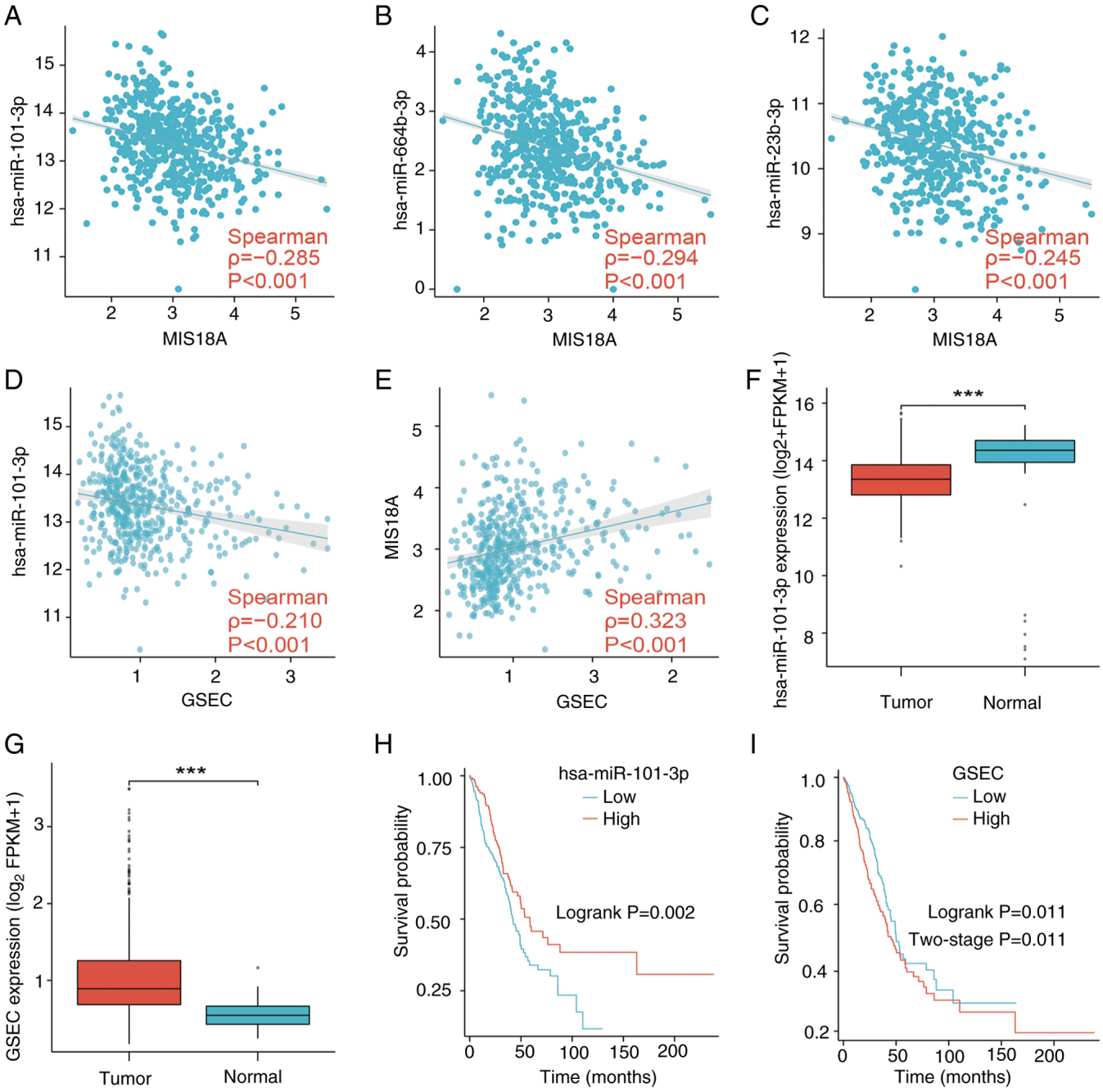

Figure 8. Establishment of the ceRNA network of MIS18A in LUAD. (A-C) Correlation analysis between three predicted miRNAs and MIS18A. (D) Correlation analysis between hsa-miR-101-3p and the predicted lncRNA, GSEC. (E) Correlation analysis between MIS18A and the predicted lncRNA, GSEC. Differential expression analysis of (F) hsa-miR-101-3p and (G) GSEC expression in LUAD. Survival analysis of (H) hsa-miR-101-3p and (I) GSEC in LUAD. ***P<0.001. LUAD, lung adenocarcinoma; MIS18A, MIS18 kinetochore protein A; miR, microRNA; FPKM, Fragments Per Kilobase per Million mapped reads.

their potential to enhance diagnostic accuracy and efficiency (38). Additionally, Liang *et al* (39) delved into the field of nanozyme-based clinical biomarker assays, which hold promising potential in disease diagnosis and personalized medicine. These research findings not only highlight the cutting-edge technologies shaping the landscape of cancer diagnostics but also provide valuable insights for improving disease detection.

At present, there is limited understanding of the role of MIS18A in tumors. As a critical component of the Mis18 complex, MIS18A is crucial for the intricate process of chromosome segregation and the precise positioning of the centromere protein, CENPA (9). An investigations has revealed that the deletion of MIS18A causes significant chromosomal misalignment, CENPA depletion and cell death (40). Notably, MIS18A and CENPA were significantly downregulated in a murine model of colorectal cancer, providing additional evidence that the aberrant functionality of MIS18A leads to erroneous chromosome segregation (41). These findings revealed the indispensable role of MIS18A in cellular division and provided crucial insights into its potential implications in tumorigenesis.

In the present study, a comprehensive analysis of MIS18A expression and its clinical implications in patients with LUAD

were conducted using diverse data sources and bioinformatic methods. The results revealed the upregulated expression of MIS18A in LUAD, highlighting its potential as a diagnostic marker. Additionally, upregulation of MIS18A in patients with LUAD showed a strong correlation with poor prognosis, suggesting its potential involvement in driving tumor progression. Therefore, MIS18A may function as an independent prognostic indicator of LUAD. In addition, a significant correlation was observed between MIS18A levels and immune characteristics. To further investigate the biological functions of MIS18A in LUAD, 899 genes in the turquoise module were analyzed. GO enrichment analysis confirmed the previous observations, establishing a significant association between MIS18A and processes related to cell division and chromosomes. Additionally, KEGG enrichment analysis further revealed a robust correlation between MIS18A and pathways such as neuroactive ligand-receptor interactions and the cell cycle. Notably, the chromosome 15q25.1 locus has been identified as a significant susceptibility region for lung cancer through a genome-wide association study (42). The study indicated that common genetic variations in this region may affect the structure or expression of genes involved in the neuroactive ligand-receptor interaction pathway, potentially influencing lung cancer susceptibility. Consequently, the neuroactive ligand-receptor interaction pathway has been identified as a risk factor for lung cancer development. Dysregulation of the cell cycle is a fundamental mechanism in tumor development and presents numerous potential targets for therapeutic intervention (43,44). In the present study, validation through GSEA reinforced these findings and suggested the potential involvement of MIS18A in processes related to the immune system. In summary, the functional enrichment analysis results highlighted the significant involvement of MIS18A in the initiation and progression of LUAD.

In the present study, WGCNA and PPI network analysis identified 6 hub genes in LUAD: MIS18A, HJURP, OIP5, CENPA, CENPK and CENPU. Cox regression analysis demonstrated that all these hub genes were associated with an elevated risk of LUAD. Furthermore, upregulation of each hub gene was indicative of an unfavorable prognosis in patients with LUAD, emphasizing their diagnostic significance. Prior studies have highlighted the significance of HJURP in LUAD, indicating that elevated HJURP expression is associated with poor prognosis (45,46). In addition, HJURP is known to facilitate tumor cell proliferation, migration and invasion via the Wnt/β-catenin signaling pathway (47). OIP5, a member of the cancer testis antigen family (48), plays a pivotal role in the structure and function of kinetochores and centromeric regions (49). Associations with the mutant genes TP53, SMARCA4 and SCN1A suggest potential pathogenic roles for OIP5 in the development of LUAD (50). Additionally, components of the CENPA-nucleosome associated complex, such as CENPA and CENPU, are essential for the development and evolution of LUAD (51,52). The upregulation of CENPK in LUAD tissues and cells has also been associated with increased cell viability, migration, invasion and epithelial-mesenchymal transition (53,54). These findings collectively reinforce the pivotal roles of the identified hub genes, including MIS18A, in driving LUAD progression, and provide additional evidence of its impact on disease progression.

The TME plays a crucial role in tumor development by influencing key processes such as growth, invasion, metastasis and immune evasion (55,56). The results of the present study revealed an association between elevated MIS18A expression and lower immune and stromal scores, along with increased tumor purity. The ssGSEA revealed a negative correlation between MIS18A expression and various tumor-infiltrating immune cells, including B cells, $CD4^+$ T cells, $CD8^+$ T cells, DCs, macrophages, natural killer cells, monocytes, eosinophils and mast cells. Notably, among the cytotoxic T lymphocytes, $CD8^+$ T cells have emerged as the primary driving force in the immune response against cancer, owing to their unique ability to directly identify and eliminate malignant cells (57). Specifically, $CD8^+$ T cells recognize major histocompatibility complex class I molecules that present tumor antigens on the surface of malignant cells. Upon recognition, $CD8^+$ T cells release cytotoxic substances such as perforin, granzymes and cytokines, resulting in the elimination of the targeted tumor cells. Additionally, $CD4^+$ T cells are crucial in tumor immunity, modulating immune responses via cytokine secretion and interactions with other immune cells, fostering an environment conducive to effective immune surveillance and tumor elimination (58). DCs possess unique abilities for antigen uptake and processing, which enable the identification and internalization of various antigens, including those present on tumor cell surfaces (59). During cancer cell invasion, chemokines and their receptors orchestrate the migration of malignant cells (60). The results of the present study identified a negative correlation between MIS18A expression and several chemokines, including chemokine (C-C motif) ligand (CCL) 14, chemokine (C-X-C motif) ligand (CXCL) 16, CCL23, CCL17, CCL19 and CCL13, as well as significant associations with diverse chemokine receptors, including CX3CR, CCR6, CXCR2, CCR4 and CCR7. The activation of monocytes, macrophages and THP-1 cells is attributable to the binding of CCL14 to CCR1, CCR3 and CCR5 (61). In addition, the Wnt/β-catenin pathway has been found to be carcinogenic in various cancer types, including hepatocellular carcinoma (HCC) (62) and LUAD (63,64). Zhu *et al* (61) demonstrated the activation of the Wnt/β-catenin pathway in HCC by CCL14. By knocking down CCL14 in HCC cells, an increase in phosphorylated-GSK3β (S9) and β-catenin (S33/S37) levels was observed, leading to the upregulation of target genes of the Wnt/β-catenin pathway. This suggested a potential pathway through which CCL14 inhibits the proliferation or apoptosis of LUAD cells. Additionally, CCR7 and CCL19 have been identified as favorable prognostic factors for patients with LUAD (65). The findings of the present study therefore underscored the significant role of MIS18A in shaping the immune microenvironment within tumors, suggesting that elevated MIS18A expression suppresses cancer immunity, thereby promoting cancer progression.

Considering the functional characteristics of MIS18A in LUAD and its impact on tumor-infiltrating immune cells, the association between MIS18A expression and the sensitivity to chemotherapy and targeted therapy was analyzed in the present study. In recent years, TMB has emerged as a focal point in the study of biomarkers associated with immune checkpoint inhibitors (ICIs) (66). Despite the ongoing debate regarding its reliability as a predictive marker (67-71), elevated TMB has

been demonstrated to stimulate the generation of novel immune antigens, enhancing tumor immunogenicity and the efficacy of ICIs (72-74). In the present study, it was noted that patients with LUAD exhibiting high MIS18A expression demonstrated a heightened TMB compared with patients with low MIS18A expression, suggesting a potential link between MIS18A and the immune response to treatment. However, further experimental validation is required to confirm this finding. In addition, the results of the OncoPredict analysis suggested that patients with LUAD and elevated MIS18A expression may benefit from treatment regimens involving cisplatin, paclitaxel, erlotinib and gefitinib. At present, cisplatin-based chemotherapy is the primary treatment for lung cancer owing to the rapid growth and metabolism of tumor cells and functions, by disrupting DNA replication and transcription and causing apoptosis in tumor cells (75). Paclitaxel, an established anticancer agent, disrupts the dynamic equilibrium of tubulin proteins, promotes tubulin protein aggregation and microtubule assembly and inhibits depolymerization, thereby stabilizing microtubules and impeding cancer cell mitosis, leading to apoptosis and effectively preventing cancer cell proliferation (76). Epidermal growth factor receptor (EGFR) is a membrane-bound receptor that is widely expressed in human epidermal and stromal cells and is known for its tyrosine kinase activity. The tyrosine kinase activity of EGFR is precisely regulated in normal cells. However, gene mutations can lead to the sustained activation of EGFR and contribute to tumorigenesis (77). Gefitinib and erlotinib, first-generation small molecule EGFR tyrosine kinase inhibitor targeted drugs extensively used in clinical settings for patients with advanced LUAD, have demonstrated promising efficacy (78,79). Gefitinib and erlotinib act by effectively binding to EGFR, inhibiting tyrosine kinase activity, blocking downstream signal transduction, suppressing angiogenesis and inducing apoptosis in tumor cells (80,81).

To validate the findings regarding the role MIS18A in LUAD, a series of cell experiments were also conducted in the present study. MIS18A knockdown significantly reduced the viability, migration and invasion of LUAD cells, highlighting its crucial role in promoting cell viability and potentially enhancing the metastatic capacity of tumor cells. These results emphasized the potential of MIS18A as a novel predictive biomarker of LUAD.

The ceRNA regulatory networks are widely acknowledged as crucial post-transcriptional regulators of gene expression. Mounting evidence indicates that ceRNA regulatory networks contribute to the regulation of various biological processes, particularly tumorigenesis (82-84). In the present study, the potential miRNAs that target MIS18A were initially predicted. A marked decrease in hsa-miR-101-3p levels was noted, which was inversely related to MIS18A expression, indicating a favorable OS in LUAD. Notably, hsa-miR-101-3p serves as a biomarker for various cancer types, including bladder cancer (85), prostate cancer (86), HCC (87) and colorectal cancer (88). Additionally, the potential upstream lncRNAs that may regulate hsa-miR-101-3p expression was predicted in the present study. The results demonstrated a significant upregulation of GSEC, which exhibited a positive correlation with MIS18A expression and was associated with a poor OS in LUAD. Existing data indicate that GSEC plays a notable role in carcinogenesis by affecting multiple signaling pathways across various cancer types, including LUAD (89), triple negative breast cancer (90) and osteosarcoma (91). However, to the best of our knowledge, the significance of the GSEC/hsa-miR-101-3p/MIS18A ceRNA regulatory network in LUAD has not yet been explored. The present study investigated the prognostic implications of the GSEC/hsa-miR-101-3p/MIS18A network, thereby providing a fresh perspective for LUAD treatment.

The present study has several limitations. First, although the expression levels and biological functions of MIS18A were successfully validated in LUAD cells, the efficiency of the si-MIS18A knockdown was not assessed by measuring MIS18A protein expression. Second, the potential molecular mechanisms by which MIS18A functions in tumor progression were not investigated. Further studies based on animal models are warranted to comprehensively elucidate the functional roles of MIS18A *in vivo*. Third, although the bioinformatics analyses revealed significant associations between MIS18A, immune infiltration and chemokines, these findings lacked experimental validation *in vitro*. In future, investigations will focus on the molecular mechanisms and immunoregulatory functions of MIS18A in LUAD.

In summary, the results of the present study suggested that MIS18A may serve as a potential diagnostic and prognostic marker in patients with LUAD. Furthermore, MIS18A has the potential to influence the biological activity of immune cells, affect the cell cycle and mitigate clinical drug resistance, suggesting its potential role in tumor immunotherapy. Notably, the experimental knockdown of MIS18A resulted in a significant reduction in cell viability, migration and invasion, emphasizing the potential of MIS18A as a biomarker and possible therapeutic target for LUAD.

Acknowledgements

Not applicable.

Funding

No funding was received.

Availability of data and materials

The data generated in the present study may be requested from the corresponding author.

Authors' contributions

YZ contributed to the conceptualization of the present study, methodology, software (coding and implementing data analysis tools), investigation (conducting and designing experiments), validation, data curation and writing of the original manuscript draft. ZL contributed to the conceptualization of the present study, methodology, investigation (data collection and experimental execution), validation and data curation. ZW contributed to the methodology, software (coding and maintaining analysis software), investigation (performing laboratory experiments) and validation. TZ contributed to the software (software testing and debugging), validation and investigation (sample analysis and data collection). LD

contributed to the methodology and investigation (conducting sample analyses). GL contributed to the investigation (data gathering and preliminary analysis) and reviewing and editing the manuscript. HP contributed to the investigation (participating in experimental work) and reviewing and editing the manuscript. HL contributed to the design and optimization of experimental methodologies, and the reviewing and editing of the manuscript. YW contributed to the organization and management of data (systematically collecting, cleaning, and preparing the data to ensure its integrity and readiness for analysis), the reviewing and editing of the manuscript, supervision of the overall research project, securing funding, and project administration. YZ and YW confirm the authenticity of all the raw data and revised the final version of the manuscript. All authors read and approved the final version of the manuscript.

Ethics approval and consent to participate

The research protocol and the process of collecting human samples received approval from The Medical Ethics Committee of The First Affiliated Hospital of Guangxi Medical University (Nanning, China; approval no. 2023-E508-01). All participants provided written informed consent.

Patient consent for publication

Not applicable.

Competing interests

The authors declare that they have no competing interests.

References

1. Sung H, Ferlay J, Siegel RL, Laversanne M, Soerjomataram I, Jemal A and Bray F: Global cancer statistics 2020: GLOBOCAN estimates of incidence and mortality worldwide for 36 cancers in 185 countries. CA Cancer J Clin 71: 209-249, 2021.
2. Zhang W, Zhang R, Zeng Y, Li Y, Chen Y, Zhou J, Zhang Y, Wang A, Zhu J, Liu Z, *et al*: ALCAP2 inhibits lung adenocarcinoma cell proliferation, migration and invasion via the ubiquitination of β-catenin by upregulating the E3 ligase NEDD4L. Cell Death Dis 12: 755, 2021.
3. Kim JW, Marquez CP, Kostyrko K, Koehne AL, Marini K, Simpson DR, Lee AG, Leung SG, Sayles LC, Shrager J, *et al*: Antitumor activity of an engineered decoy receptor targeting CLCF1-CNTFR signaling in lung adenocarcinoma. Nat Med 25: 1783-1795, 2019.
4. Oudkerk M, Liu S, Heuvelmans MA, Walter JE and Field JK: Lung cancer LDCT screening and mortality reduction-evidence, pitfalls and future perspectives. Nat Rev Clin Oncol 18: 135-151, 2021.
5. Fang C, Liang Y, Huang Y, Jiang D, Li J, Ma H, Guo L, Jiang W and Feng Y: P3H4 promotes malignant progression of lung adenocarcinoma via interaction with EGFR. Cancers (Basel) 14: 3243, 2022.
6. Imielinski M, Berger AH, Hammerman PS, Hernandez B, Pugh TJ, Hodis E, Cho J, Suh J, Capelletti M, Sivachenko A, *et al*: Mapping the hallmarks of lung adenocarcinoma with massively parallel sequencing. Cell 150: 1107-1120, 2012.
7. Pan D, Klare K, Petrovic A, Take A, Walstein K, Singh P, Rondelet A, Bird AW and Musacchio A: CDK-regulated dimerization of M18BP1 on a Mis18 hexamer is necessary for CENP-A loading. Elife 6: e23352, 2017.
8. Fujita Y, Hayashi T, Kiyomitsu T, Toyoda Y, Kokubu A, Obuse C and Yanagida M: Priming of centromere for CENP-A recruitment by human hMis18alpha, hMis18beta, and M18BP1. Dev Cell 12: 17-30, 2007.
9. Nardi IK, Zasadzińska E, Stellfox ME, Knippler CM and Foltz DR: Licensing of centromeric chromatin assembly through the Mis18α-Mis18β heterotetramer. Mol Cell 61: 774-787, 2016.
10. Sullivan KF, Hechenberger M and Masri K: Human CENP-A contains a histone H3 related histone fold domain that is required for targeting to the centromere. J Cell Biol 127: 581-592, 1994.
11. Liu WT, Wang Y, Zhang J, Ye F, Huang XH, Li B and He QY: A novel strategy of integrated microarray analysis identifies CENPA, CDK1 and CDC20 as a cluster of diagnostic biomarkers in lung adenocarcinoma. Cancer Lett 425: 43-53, 2018.
12. Kim IS, Lee M, Park KC, Jeon Y, Park JH, Hwang EJ, Jeon TI, Ko S, Lee H, Baek SH and Kim KI: Roles of Mis18α in epigenetic regulation of centromeric chromatin and CENP-A loading. Mol Cell 46: 260-273, 2012.
13. Sun SY, Hu XT, Yu XF, Zhang YY, Liu XH, Liu YH, Wu SH, Li YY, Cui SX and Qu XJ: Nuclear translocation of ATG5 induces DNA mismatch repair deficiency (MMR-D)/microsatellite instability (MSI) via interacting with Mis18α in colorectal cancer. Br J Pharmacol 178: 2351-2369, 2021.
14. Goldman MJ, Craft B, Hastie M, Repečka K, McDade F, Kamath A, Banerjee A, Luo Y, Rogers D, Brooks AN, *et al*: Visualizing and interpreting cancer genomics data via the Xena platform. Nat Biotechnol 38: 675-678, 2020.
15. Rousseaux S, Debernardi A, Jacquiau B, Vitte AL, Vesin A, Nagy-Mignotte H, Moro-Sibilot D, Brichon PY, Lantuejoul S, Hainaut P, *et al*: Ectopic activation of germline and placental genes identifies aggressive metastasis-prone lung cancers. Sci Transl Med 5: 186ra166, 2013.
16. Landi MT, Dracheva T, Rotunno M, Figueroa JD, Liu H, Dasgupta A, Mann FE, Fukuoka J, Hames M, Bergen AW, *et al*: Gene expression signature of cigarette smoking and its role in lung adenocarcinoma development and survival. PLoS One 3: e1651, 2008.
17. Wei TYW, Hsia JY, Chiu SC, Su LJ, Juan CC, Lee YC, Chen JM, Chou HY, Huang JY, Huang HM and Yu CT: Methylosome protein 50 promotes androgen- and estrogen-independent tumorigenesis. Cell Signal 26: 2940-2950, 2014.
18. Li T, Fan J, Wang B, Traugh N, Chen Q, Liu JS, Li B and Liu XS: TIMER: A web server for comprehensive analysis of tumor-infiltrating immune cells. Cancer Res 77: e108-e110, 2017.
19. Uhlén M, Fagerberg L, Hallström BM, Lindskog C, Oksvold P, Mardinoglu A, Sivertsson Å, Kampf C, Sjöstedt E, Asplund A, *et al*: Proteomics. Tissue-based map of the human proteome. Science 347: 1260419, 2015.
20. Chandrashekar DS, Bashel B, Balasubramanya SAH, Creighton CJ, Ponce-Rodriguez I, Chakravarthi BVSK and Varambally S: UALCAN: A portal for facilitating tumor subgroup gene expression and survival analyses. Neoplasia 19: 649-658, 2017.
21. Therneau T: A package for survival analysis in R. R package version 3.6-4, 2024.
22. Kassambara A, Kosinski M and Biecek P: Survminer: Drawing survival curves using 'ggplot2'. R package version 0.4.9, 2021.
23. Tang Z, Li C, Kang B, Gao G, Li C and Zhang Z: GEPIA: A web server for cancer and normal gene expression profiling and interactive analyses. Nucleic Acids Res 45: W98-W102, 2017.
24. Love MI, Huber W and Anders S: Moderated estimation of fold change and dispersion for RNA-seq data with DESeq2. Genome Biol 15: 550, 2014.
25. Langfelder P and Horvath S: WGCNA: An R package for weighted correlation network analysis. BMC Bioinformatics 9: 559, 2008.
26. Mostafavi S, Ray D, Warde-Farley D, Grouios C and Morris Q: GeneMANIA: A real-time multiple association network integration algorithm for predicting gene function. Genome Biol 9 (Suppl 1): S4, 2008.
27. Yoshihara K, Shahmoradgoli M, Martínez E, Vegesna R, Kim H, Torres-Garcia W, Treviño V, Shen H, Laird PW, Levine DA, *et al*: Inferring tumour purity and stromal and immune cell admixture from expression data. Nat Commun 4: 2612, 2013.
28. Hänzelmann S, Castelo R and Guinney J: GSVA: Gene set variation analysis for microarray and RNA-seq data. BMC Bioinformatics 14: 7, 2013.
29. Mayakonda A, Lin DC, Assenov Y, Plass C and Koeffler HP: Maftools: Efficient and comprehensive analysis of somatic variants in cancer. Genome Res 28: 1747-1756, 2018.
30. Yang W, Soares J, Greninger P, Edelman EJ, Lightfoot H, Forbes S, Bindal N, Beare D, Smith JA, Thompson IR, *et al*: Genomics of drug sensitivity in cancer (GDSC): A resource for therapeutic biomarker discovery in cancer cells. Nucleic Acids Res 41 (Database Issue): D955-D961, 2013.

31. Stridfeldt F, Cavallaro S, Hååg P, Lewensohn R, Linnros J, Viktorsson K and Dev A: Analyses of single extracellular vesicles from non-small lung cancer cells to reveal effects of epidermal growth factor receptor inhibitor treatments. Talanta 259: 124553, 2023.
32. Zhang K, Zhang L, Mi Y, Tang Y, Ren F, Liu B, Zhang Y and Zheng P: A ceRNA network and a potential regulatory axis in gastric cancer with different degrees of immune cell infiltration. Cancer Sci 111: 4041-4050, 2020.
33. Song YX, Sun JX, Zhao JH, Yang YC, Shi JX, Wu ZH, Chen XW, Gao P, Miao ZF and Wang ZN: Non-coding RNAs participate in the regulatory network of CLDN4 via ceRNA mediated miRNA evasion. Nat Commun 8: 289, 2017.
34. Salmena L, Poliseno L, Tay Y, Kats L and Pandolfi PP: A ceRNA hypothesis: The Rosetta Stone of a hidden RNA language? Cell 146: 353-358, 2011.
35. Malhotra J, Malvezzi M, Negri E, La Vecchia C and Boffetta P: Risk factors for lung cancer worldwide. Eur Respir J 48: 889-902, 2016.
36. Cucchiara F, Petrini I, Romei C, Crucitta S, Lucchesi M, Valleggi S, Scavone C, Capuano A, De Liperi A, Chella A, *et al*: Combining liquid biopsy and radiomics for personalized treatment of lung cancer patients. State of the art and new perspectives. Pharmacol Res 169: 105643, 2021.
37. Wang L, Zhang M, Pan X, Zhao M, Huang L, Hu X, Wang X, Qiao L, Guo Q, Xu W, *et al*: Integrative serum metabolic fingerprints based multi-modal platforms for lung adenocarcinoma early detection and pulmonary nodule classification. Adv Sci (Weinh) 9: e2203786, 2022.
38. Chen X, Shu W, Zhao L and Wan J: Advanced mass spectrometric and spectroscopic methods coupled with machine learning for in vitro diagnosis. VIEW 4: 20220038, 2023.
39. Liang D, Wang Y and Qian K: Nanozymes: Applications in clinical biomarker detection. Interdiscip Med 1: e20230020, 2023.
40. Baumann K: Keeping centromeric identity. Nat Rev Mol Cell Biol 13: 340, 2012.
41. Pussila M, Törönen P, Einarsdottir E, Katayama S, Krjutškov K, Holm L, Kere J, Peltomäki P, Mäkinen MJ, Linden J and Nyström M: Mlh1 deficiency in normal mouse colon mucosa associates with chromosomally unstable colon cancer. Carcinogenesis 39: 788-797, 2018.
42. Ji X, Bossé Y, Landi MT, Gui J, Xiao X, Qian D, Joubert P, Lamontagne M, Li Y, Gorlov I, *et al*: Identification of susceptibility pathways for the role of chromosome 15q25.1 in modifying lung cancer risk. Nat Commun 9: 3221, 2018.
43. Carroll B and Korolchuk VI: Nutrient sensing, growth and senescence. FEBS J 285: 1948-1958, 2018.
44. Kamal MA, Al-Zahrani MH, Khan SH, Al-Subhi HA, Kuerban A, Aslam M, Al-Abbasi FA and Anwar F: Tubulin proteins in cancer resistance: A review. Curr Drug Metab 21: 178-185, 2020.
45. Chen L, Zeng C, Yan L, Liao W, Zhen C and Yao J: Prognostic value of holliday junction-recognizing protein and its correlation with immune infiltrates in lung adenocarcinoma. Oncol Lett 24: 232, 2022.
46. Yin Q, Chen W, Zhang C and Wei Z: A convolutional neural network model for survival prediction based on prognosis-related cascaded Wx feature selection. Lab Invest 102: 1064-1074, 2022.
47. Wei Y, Ouyang GL, Yao WX, Zhu YJ, Li X, Huang LX, Yang XW and Jiang WJ: Knockdown of HJURP inhibits non-small cell lung cancer cell proliferation, migration, and invasion by repressing Wnt/β-catenin signaling. Eur Rev Med Pharmacol Sci 23: 3847-3856, 2019.
48. Afsharpad M, Nowroozi MR, Mobasheri MB, Ayati M, Nekoohesh L, Saffari M, Zendehdel K and Modarressi MH: Cancer-testis antigens as new candidate diagnostic biomarkers for transitional cell carcinoma of bladder. Pathol Oncol Res 25: 191-199, 2019.
49. Naetar N, Hutter S, Dorner D, Dechat T, Korbei B, Gotzmann J, Beug H and Foisner R: LAP2alpha-binding protein LINT-25 is a novel chromatin-associated protein involved in cell cycle exit. J Cell Sci 120: 737-747, 2007.
50. Abdel-Maksoud MA, Hassan F, Mubarik U, Mubarak A, Farrag MA, Alghamdi S, Atuahene SA, Almekhlafi S and Aufy M: An in-silico approach leads to explore six genes as a molecular signatures of lung adenocarcinoma. Am J Cancer Res 13: 727-757, 2023.
51. Zhou H, Bian T, Qian L, Zhao C, Zhang W, Zheng M, Zhou H, Liu L, Sun H, Li X, *et al*: Prognostic model of lung adenocarcinoma constructed by the CENPA complex genes is closely related to immune infiltration. Pathol Res Pract 228: 153680, 2021.
52. Wu Q, Chen YF, Fu J, You QH, Wang SM, Huang X, Feng XJ and Zhang SH: Short hairpin RNA-mediated down-regulation of CENP-A attenuates the aggressive phenotype of lung adenocarcinoma cells. Cell Oncol (Dordr) 37: 399-407, 2014.
53. Wang Y, Wang Y, Ren C, Wang H, Zhang Y and Xiu Y: Upregulation of centromere protein K is crucial for lung adenocarcinoma cell viability and invasion. Adv Clin Exp Med 30: 691-699, 2021.
54. Lai H, Wen X, Peng Y and Zhang L: Identification of stem cell-related gene markers by comprehensive transcriptome analysis to predict the prognosis and immunotherapy of lung adenocarcinoma. Curr Stem Cell Res Ther 19: 743-754, 2024.
55. Monteran L, Zait Y and Erez N: It's all about the base: Stromal cells are central orchestrators of metastasis. Trends Cancer 10: 208-229, 2024.
56. Gao D, Fang L, Liu C, Yang M, Yu X, Wang L, Zhang W, Sun C and Zhuang J: Microenvironmental regulation in tumor progression: Interactions between cancer-associated fibroblasts and immune cells. Biomed Pharmacother 167: 115622, 2023.
57. Hebeisen M, Oberle SG, Presotto D, Speiser DE, Zehn D and Rufer N: Molecular insights for optimizing T cell receptor specificity against cancer. Front Immunol 4: 154, 2013.
58. Speiser DE, Chijioke O, Schaeuble K and Münz C: $CD4^+$ T cells in cancer. Nat Cancer 4: 317-329, 2023.
59. Cardenas MA, Prokhnevska N and Kissick HT: Organized immune cell interactions within tumors sustain a productive T-cell response. Int Immunol 33: 27-37, 2021.
60. Laurent V, Guérard A, Mazerolles C, Le Gonidec S, Toulet A, Nieto L, Zaidi F, Majed B, Garandeau D, Socrier Y, *et al*: Periprostatic adipocytes act as a driving force for prostate cancer progression in obesity. Nat Commun 7: 10230, 2016.
61. Zhu M, Xu W, Wei C, Huang J, Xu J, Zhang Y, Zhao Y, Chen J, Dong S, Liu B and Liang C: CCL14 serves as a novel prognostic factor and tumor suppressor of HCC by modulating cell cycle and promoting apoptosis. Cell Death Dis 10: 796, 2019.
62. Chen J, Rajasekaran M, Xia H, Zhang X, Kong SN, Sekar K, Seshachalam VP, Deivasigamani A, Goh BK, Ooi LL, *et al*: The microtubule-associated protein PRC1 promotes early recurrence of hepatocellular carcinoma in association with the Wnt/β-catenin signalling pathway. Gut 65: 1522-1534, 2016.
63. Jiang N, Zou C, Zhu Y, Luo Y, Chen L, Lei Y, Tang K, Sun Y, Zhang W, Li S, *et al*: HIF-1α-regulated miR-1275 maintains stem cell-like phenotypes and promotes the progression of LUAD by simultaneously activating Wnt/β-catenin and Notch signaling. Theranostics 10: 2553-2570, 2020.
64. Cao Y, Geng J, Wang X, Meng Q, Xu S, Lang Y, Zhou Y, Qi L, Wang Z, Wei Z, *et al*: RNA-binding motif protein 10 represses tumor progression through the Wnt/β-catenin pathway in lung adenocarcinoma. Int J Biol Sci 18: 124-139, 2022.
65. Itakura M, Terashima Y, Shingyoji M, Yokoi S, Ohira M, Kageyama H, Matui Y, Yoshida Y, Ashinuma H, Moriya Y, *et al*: High CC chemokine receptor 7 expression improves postoperative prognosis of lung adenocarcinoma patients. Br J Cancer 109: 1100-1108, 2013.
66. Choucair K, Morand S, Stanbery L, Edelman G, Dworkin L and Nemunaitis J: TMB: A promising immune-response biomarker, and potential spearhead in advancing targeted therapy trials. Cancer Gene Ther 27: 841-853, 2020.
67. Hellmann MD, Nathanson T, Rizvi H, Creelan BC, Sanchez-Vega F, Ahuja A, Ni A, Novik JB, Mangarin LMB, Abu-Akeel M, *et al*: Genomic features of response to combination immunotherapy in patients with advanced non-small-cell lung cancer. Cancer Cell 33: 843-852.e4, 2018.
68. Samstein RM, Lee CH, Shoushtari AN, Hellmann MD, Shen R, Janjigian YY, Barron DA, Zehir A, Jordan EJ, Omuro A, *et al*: Tumor mutational load predicts survival after immunotherapy across multiple cancer types. Nat Genet 51: 202-206, 2019.
69. Goodman AM, Kato S, Bazhenova L, Patel SP, Frampton GM, Miller V, Stephens PJ, Daniels GA and Kurzrock R: Tumor mutational burden as an independent predictor of response to immunotherapy in diverse cancers. Mol Cancer Ther 16: 2598-2608, 2017.
70. Rizvi H, Sanchez-Vega F, La K, Chatila W, Jonsson P, Halpenny D, Plodkowski A, Long N, Sauter JL, Rekhtman N, *et al*: Molecular determinants of response to anti-programmed cell death (PD)-1 and anti-programmed death-ligand 1 (PD-L1) blockade in patients with non-small-cell lung cancer profiled with targeted next-generation sequencing. J Clin Oncol 36: 633-641, 2018.

71. Hellmann MD, Ciuleanu TE, Pluzanski A, Lee JS, Otterson GA, Audigier-Valette C, Minenza E, Linardou H, Burgers S, Salman P, *et al*: Nivolumab plus ipilimumab in lung cancer with a high tumor mutational burden. N Engl J Med 378: 2093-2104, 2018.
72. Havel JJ, Chowell D and Chan TA: The evolving landscape of biomarkers for checkpoint inhibitor immunotherapy. Nat Rev Cancer 19: 133-150, 2019.
73. Jardim DL, Goodman A, de Melo Gagliato D and Kurzrock R: The challenges of tumor mutational burden as an immunotherapy biomarker. Cancer Cell 39: 154-173, 2021.
74. Chan TA, Yarchoan M, Jaffee E, Swanton C, Quezada SA, Stenzinger A and Peters S: Development of tumor mutation burden as an immunotherapy biomarker: Utility for the oncology clinic. Ann Oncol 30: 44-56, 2019.
75. Yang Y, Adebali O, Wu G, Selby CP, Chiou YY, Rashid N, Hu J, Hogenesch JB and Sancar A: Cisplatin-DNA adduct repair of transcribed genes is controlled by two circadian programs in mouse tissues. Proc Natl Acad Sci USA 115: E4777-E4785, 2018.
76. Zhu L and Chen L: Progress in research on paclitaxel and tumor immunotherapy. Cell Mol Biol Lett 24: 40, 2019.
77. Ahmadi A, Mohammadnejadi E and Razzaghi-Asl N: Gefitinib derivatives and drug-resistance: A perspective from molecular dynamics simulations. Comput Biol Med 163: 107204, 2023.
78. Zou J, Lan H, Li W, Xie S, Tong Z, Song X and Wang C: Comprehensive analysis of circular RNA expression profiles in gefitinib-resistant lung adenocarcinoma patients. Technol Cancer Res Treat 21: 15330338221139167, 2022.
79. Zhang Q and Xu K: Advances in the research of autophagy in EGFR-TKI treatment and resistance in lung cancer. Zhongguo Fei Ai Za Zhi 19: 607-614, 2016 (In Chinese).
80. Fukuoka M, Wu YL, Thongprasert S, Sunpaweravong P, Leong SS, Sriuranpong V, Chao TY, Nakagawa K, Chu DT, Saijo N, *et al*: Biomarker analyses and final overall survival results from a phase III, randomized, open-label, first-line study of gefitinib versus carboplatin/paclitaxel in clinically selected patients with advanced non-small-cell lung cancer in Asia (IPASS). J Clin Oncol 29: 2866-2874, 2011.
81. Zhou C, Wu YL, Chen G, Feng J, Liu XQ, Wang C, Zhang S, Wang J, Zhou S, Ren S, *et al*: Erlotinib versus chemotherapy as first-line treatment for patients with advanced EGFR mutation-positive non-small-cell lung cancer (OPTIMAL, CTONG-0802): A multicentre, open-label, randomised, phase 3 study. Lancet Oncol 12: 735-742, 2011.
82. Chen C, Wan M, Peng X, Zhang Q and Liu Y: GPR37-centered ceRNA network contributes to metastatic potential in lung adenocarcinoma: Evidence from high-throughput sequencing. Transl Oncol 39: 101819, 2024.
83. Wu X, Sui Z, Zhang H, Wang Y and Yu Z: Integrated analysis of lncRNA-Mediated ceRNA network in lung adenocarcinoma. Front Oncol 10: 554759, 2020.
84. Feng W, Gong H, Wang Y, Zhu G, Xue T, Wang Y and Cui G: circIFT80 functions as a ceRNA of miR-1236-3p to promote colorectal cancer progression. Mol Ther Nucleic Acids 18: 375-387, 2019.
85. Rao X, Cao H, Yu Q, Ou X, Deng R and Huang J: NEAT1/MALAT1/XIST/PKD-Hsa-Mir-101-3p-DLGAP5 axis as a novel diagnostic and prognostic biomarker associated with immune cell infiltration in bladder cancer. Front Genet 13: 892535, 2022.
86. Duca RB, Massillo C, Dalton GN, Farré PL, Graña KD, Gardner K and De Siervi A: MiR-19b-3p and miR-101-3p as potential biomarkers for prostate cancer diagnosis and prognosis. Am J Cancer Res 11: 2802-2820, 2021.
87. Chen Z, Lin X, Wan Z, Xiao M, Ding C, Wan P, Li Q and Zheng S: High expression of EZH2 mediated by ncRNAs correlates with poor prognosis and tumor immune infiltration of hepatocellular carcinoma. Genes (Basel) 13: 876, 2022.
88. Tao L, Xu C, Shen W, Tan J, Li L, Fan M, Sun D, Lai Y and Cheng H: HIPK3 inhibition by exosomal hsa-miR-101-3p is related to metabolic reprogramming in colorectal cancer. Front Oncol 11: 758336, 2022.
89. Song J, Sun Y, Cao H, Liu Z, Xi L, Dong C, Yang R and Shi Y: A novel pyroptosis-related lncRNA signature for prognostic prediction in patients with lung adenocarcinoma. Bioengineered 12: 5932-5949, 2021.
90. Zhang J, Du C, Zhang L, Wang Y, Zhang Y and Li J: lncRNA GSEC promotes the progression of triple negative breast cancer (TNBC) by targeting the miR-202-5p/AXL axis. Onco Targets Ther 14: 2747-2759, 2021.
91. Liu R, Ju C, Zhang F, Tang X, Yan J, Sun J, Lv B, Guo Y, Liang Y, Lv XB and Zhang Z: LncRNA GSEC promotes the proliferation, migration and invasion by sponging miR-588/EIF5A2 axis in osteosarcoma. Biochem Biophys Res Commun 532: 300-307, 2020.